energies

MDPI

Article

Heat Transfer and Fluid Flow Characteristics in a Micro Heat Exchanger Employing Warm Nanofluids for Cooling of Electronic Components

Mahdi Mokrane [1] and Mahmoud Bourouis [2,*]

[1] Centre de Développement des Énergies Renouvelables (CDER), Unité de Développement des Équipements Solaires (UDES), Tipaza 42004, Algeria; mok.mehdi@gmail.com
[2] Department of Mechanical Engineering, Universitat Rovira i Virgili, Av. Països Catalans No. 26, 43007 Tarragona, Spain
* Correspondence: mahmoud.bourouis@urv.cat

Abstract: The heat transfer enhancement and hydrodynamic characteristics of nanofluid use in a micro heat exchanger is investigated for cooling electronic components working in hot climatic conditions. The cooling fluid employed was water and TiO_2 nanoparticles at mass concentrations of 1% and 5%, the Reynolds numbers ranged from 400 to 2000, and the inlet temperatures ranged between 35 °C and 65 °C. At a nanofluid inlet temperature of 55 °C and a nanoparticle concentration of 1%, the Nusselt number increased by 23% up to 54% as the Reynolds number varied between 400 and 2000. At a nanoparticle concentration of 5%, the percentages that correspondingly enhanced the Nusselt number were 32% and 63%. The temperature of the electronic heating component decreased by 4.6–5.2 °C when the nanofluid concentration was increased from 0 to 5% at a Reynolds number of 400 and a nanofluid inlet temperature of 35 °C. Small increments in the pressure drop of about 6% and 13% were observed at nanofluid concentrations of 1% and 5%, respectively. With nanoparticle concentrations of 1% and 5%, a Reynolds number of 2000, and a nanofluid inlet temperature of 35 °C, performance evaluation criterion (PEC) values of 1.36 and 1.45 were obtained. When the nanofluid inlet temperature increased to 65 °C, the PEC parameter decreased to 1.02–1.10 for both concentrations.

Keywords: micro heat exchanger; nanofluids; cooling of electronic heating components; CFD simulation

Citation: Mokrane, M.; Bourouis, M. Heat Transfer and Fluid Flow Characteristics in a Micro Heat Exchanger Employing Warm Nanofluids for Cooling of Electronic Components. *Energies* **2024**, *17*, 2383. https://doi.org/10.3390/en17102383

Academic Editor: Artur Blaszczuk

Received: 18 April 2024
Revised: 10 May 2024
Accepted: 10 May 2024
Published: 15 May 2024

1. Introduction

The microelectronics sector, which manufactures electronic circuits, has grown quickly and has also manufactured more powerful, compact, and advantageous components for portable and fixed applications. These include data centers, electronic boxes, and cars. However, overheating of these electronic components could affect their performance and reduce their life cycles, particularly when they are used in regions suffering hot weather conditions [1]. To enhance thermal conductivity in electronic devices operating in these conditions, it is essential to apply cooling systems that can appropriately dissipate the high heat flux released. The selection and design of a specific cooling system depend mainly on the heat flux dissipated by the heating component, the climatic conditions of the site, and the energy parameter for the cooling capacity required from the system installed. Among these methods, forced convection air cooling has been the one most commonly employed to maintain the working temperature of electronic components at a safe level. This is because of its simplicity and inherent cost-effectiveness. However, this cooling system remains limited for implementation in high-performance microelectronic equipment, and, as a consequence, there is a rising interest in designing other methods of high-performance liquid cooling systems [2,3].

Single-phase microchannel heat sinks, consisting of a stream of water passing through a micro heat exchanger, are an efficient means of dissipating heat fluxes. These fluxes, usually in the order of hundreds of W/cm^2, exceed the rates that air-cooled systems are able to reach [4]. In terms of cooling efficiency, micro heat exchangers are particularly promising components for usage in small-scale and advanced applications. They are compact, light, have low energy requirements, and have a relatively low cost. Therefore, they provide vast windows of opportunity for integration into microelectronic components. The functional features of micro heat exchangers were originally explored by Tuckerman and Pease in the early 1980s [4]. This concept led to the investigation of heat transfer and fluid flow in rectangular microchannels. Microscopic channels 50 µm wide and 300 µm deep were etched in silicon, and deionized water was pushed through as the coolant. This design permitted the dissipation of 790 W/cm^2, with a temperature increase of 71 °C for a single chip. Gao et al. [5] studied the influence of channel height on the thermo-hydraulic characteristics of microchannels and minichannels. Friction factors agreed with those estimated by the conventional laminar theory, regardless of channel height. However, the authors noticed a heat transfer enhancement when the size of the channels was decreased. Mala and Li [6] performed an experimental study into how microchannel diameter variation affected the pressure drop. The authors reported significant deviations between the flow characteristics and the theoretical predictions for microchannels with a reduced diameter.

Several numerical investigations evaluated the impact of the microchannel's geometrical design on heat transfer mechanisms and flow patterns [7–13]. One of the most relevant results found that corrugated microchannels demonstrate a high potential for dissipating high heat fluxes. Other studies [14–19] are based on the tree design reported by Bejan [20]. This design is useful for selecting the best geometric layout for heat sinks to allow for maximum heat transfer between the cooling fluid and the wall of the microchannels.

Investigations are currently being carried out on the improvement in the thermophysical properties of coolants and have attracted the interest of various researchers over the last few decades [21]. The most promising technique to improve heat transfer is to employ nanofluids with metal nanoparticles in the base fluid. This mixture is more effective than conventional working fluids, such as water, ethylene glycol, or oil [22–24]. Several computational and experimental studies available in the literature are focused on the heat transfer and fluid flow of nanofluids on macro- and microscales [25–46]. Kalteh et al. [47] investigated, numerically and experimentally, the flow of alumina–water nanofluid, at a volume concentration ranging from 0% to 5%, inside a wide heat sink microchannel. The two-phase Eulerian method was utilized to model the nanofluid flow. In addition, homogeneous modeling was carried out to compare the experimental results with those of the two-phase simulation approach. The authors' numerical results demonstrated that the two-phase technique was more appropriate than the homogeneous model for modeling nanofluid flow. The maximum deviations with experimental results were 12.6% and 7.4% for the homogeneous and two-phase methods, respectively. Mohammed et al. [48] analyzed the performance of microchannel heat sinks employing Al_2O_3/water nanofluids at concentrations of 1–5%. They employed the finite volume approach, based on a hybrid discretization methodology and the SIMPLE algorithm to solve the velocity fields. The results revealed that the use of nanofluids can enhance the heat transfer in heat sink microchannels and that it was dependent on the volumetric fraction of nanoparticles dispersed in the base fluid. The authors also observed that the thermal resistance was lower for heat sink microchannels with nanofluids at a 5% nanoparticle volume fraction. TiO_2 nanoparticles have good heat transfer characteristics, are highly stable, easily available, ecologically safe, and low cost. Experimental research exploring the influence of high nanoparticle concentrations (=2%) on convective heat transfer in microchannels is very scarce. Manay and Sahin [49] studied how microchannel height and five different TiO_2 nanoparticle volume fractions of nanofluids (0.25%, 0.5%, 1.0%, 1.5%, and 2.0%) in pure water impacted the heat transfer and flow characteristics. The study indicated that a reduction in the microchannel height significantly decreased heat duties and increased pressure drop. By increasing the nanosized TiO_2 particles concentration in the base fluid, heat transfer rates increased, but there was no excessive increase in the pressure drop when compared to using pure water. Furthermore, various studies are available in the literature on the use of high concentrations of TiO_2/water nanofluids in micro heat exchangers. Martínez et al. [50] investigated numerically the effect of microchannel height on the thermal performance of a heat sink subjected to a continuous heat flow of 50 W/cm^2 at the bottom surface. The dimensions of the microchannel were 283 µm in width and 50 mm in length, with three different heights (800 µm, 600 µm, and 400 µm). A laminar three-dimensional flow study was carried out using water and TiO_2/water nanofluids at weight concentrations of 1 wt% and 3 wt%, with Reynolds numbers ranging from 200 to 1200. The authors concluded that both the use of nanoparticles and the reduction in the microchannel height improved the heat transfer at a low Reynolds number of 200. The maximum increase obtained was 19.7% with a nanoparticle concentration of 3%.

To determine the heat transfer rate and friction factor, Nitiapiruk et al. [51] investigated the effects of TiO_2/water nanofluids, at volume concentration of 0.5%, 1%, and 2%, in a microchannel heat sink with 40 flowing channels. The length, width, and height of each channel were 40 mm, 500 µm, and 800 µm, respectively. The authors reported that the use of nanoparticles at a volume fraction of 2% with minimum heat flux and Reynolds number values was more suitable than other volume fractions. Heydari et al. [52] investigated the effect of a rib design on the heat transfer characteristics and laminar flow for the nanofluid TiO_2/water in a three-dimensional rectangular microchannel at volume fractions of 0%, 2%, and 4%. The results indicated that the ribs significantly affected the pattern of fluid flow; however, it also varied depending on the Reynolds number of the flow.

All of these studies reported a significant enhancement in the heat transfer with the addition of nanofluids, which was dependent on the nanoparticles concentration. The heat transfer improvement ranged from 12.6% to 53% depending on the nanoparticle concentration and microchannel geometry. The results also showed the importance of considering the thermophysical properties of nanofluids, which differ from those of water depending on the concentration of suspended nanoparticles.

The present study involved the use of titanium dioxide (TiO_2) nanoparticles in a micro heat exchanger to investigate how this could enhance heat transfer for the cooling of electronic components. There is scarce information in the open literature on the impact of using both micro heat exchangers and nanofluids for the cooling of electronic components at high coolant inlet temperatures. Experiments and numerical simulations were conducted to explore how different parameters, such as the inlet temperature of the hot nanofluids, Reynolds number, and concentration of nanoparticles, affect heat transfer enhancement in the cooling of an electronic heating component. The results of this study could be very useful for the design of efficient cooling systems for electronic devices that operate at high temperatures. The use of nanofluids in micro heat exchangers can improve heat transfer performance and reduce energy consumption, which is essential in many industrial electronics applications.

2. Geometry of the Experimental Setup and Measurement Procedure

2.1. Geometry

The micro heat exchanger consisted of two collectors and a micro heat sink, as illustrated in Figure 1a. A cross-section of the heat sink is shown in Figure 1b. It was made up of 17 aluminum microchannels, each measuring 40 mm in length and having a rectangular cross-section that is 1 mm in height and 0.7 mm in width.

Table 1 summarizes the main geometrical characteristics of the micro heat exchanger. Aluminum was used as the manufacturing material because of its resistance to corrosion and its high durability. The fluid circulating in the microchannels was distributed using two aluminum circular distributors, each 5 mm in diameter, with the first at the inflow and the second at the outflow.

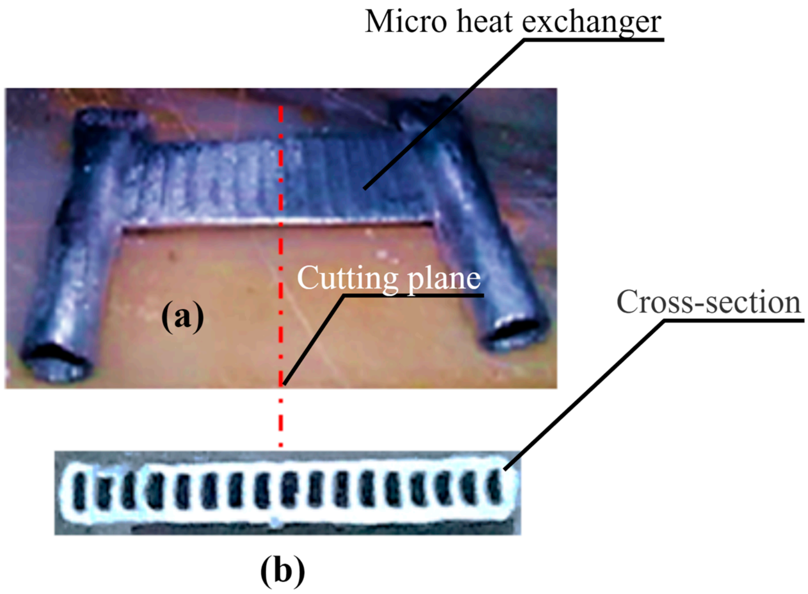

Figure 1. Test module: (**a**) micro heat exchanger; (**b**) microchannels.

Table 1. Geometric parameters of the micro heat exchanger shown in Figure 2.

Geometric Parameter	Dimension (mm)/Number (-)
Heat sink width (W)	16
Heat sink height (H)	1.63
Heat sink length (L_{mc})	40
Microchannel width (W_{mc})	0.7
Microchannel height (H_{mc})	1
Half thickness of the solid (e_s)	0.35
Thickness of fins (e)	0.25
Collector tube length (L_c)	40
Hydraulic diameter (D_h)	0.8
Collector tube diameter (D_c)	5
Number of channels (N)	17

2.2. Experimental Apparatus

This section presents the setup and methodology employed to perform the experiments. Figure 3 depicts the test section, consisting of a heating element 40 mm long, 25 mm wide, and 4 mm thick. Polyurethane insulation was employed to reduce heat losses. A thin layer of thermal paste (Arctic MX-4, Braunschweig, Germany) with a thermal conductivity of 8.5 W/m.K was also applied between the micro heat exchanger and the heating element. Heat was generated by transmitting an electric current through the heating element (Joule effect). The heat generated $(\dot{P})$ was determined using Equation (1):

$$\dot{P} = I \times \dot{U} \tag{1}$$

where $\dot{U}$ is the voltage across the heating component, and I is the electric current.

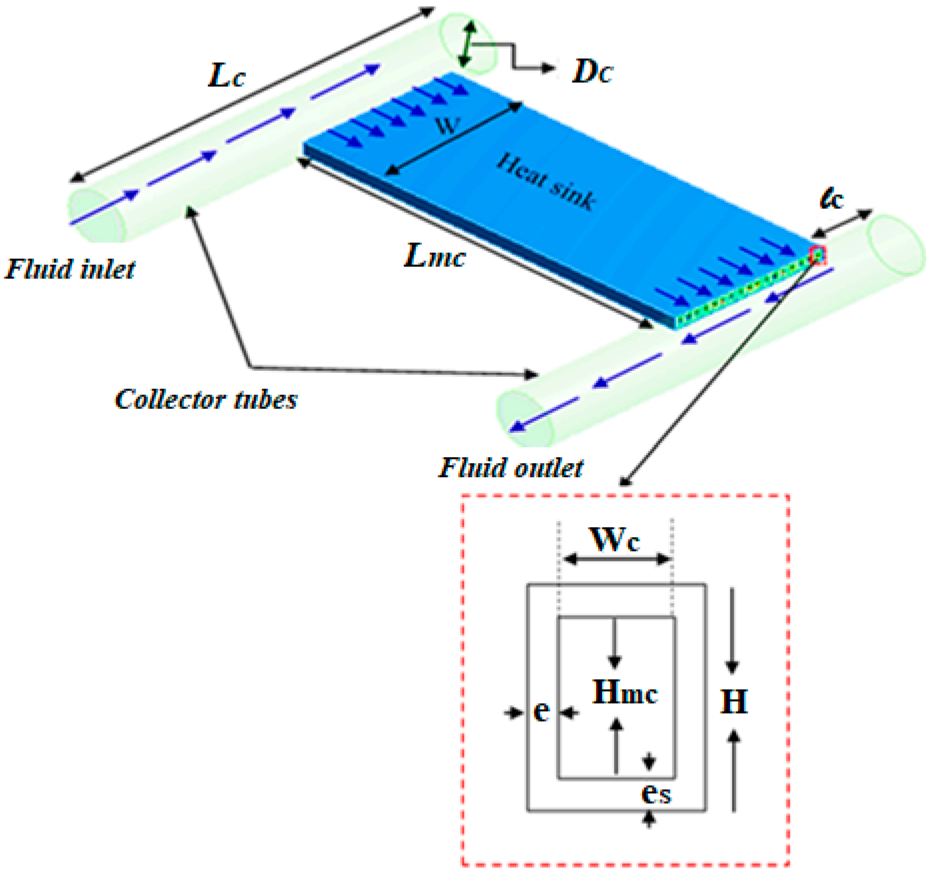

Figure 2. Schematic diagram of the micro channel heat exchanger assembly.

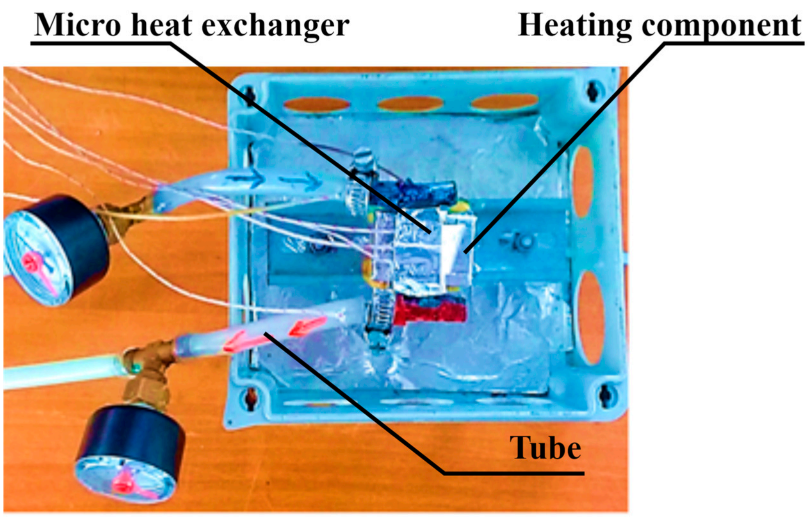

Figure 3. Experimental rig.

The experiments were carried out using the maximum voltages, which corresponded to a power supply of 100 W. This made it possible to generate a maximum temperature of 160 °C. The temperature on the heating component side was uniform.

The assembled device was fixed in the center of an 18 × 13 × 10 cm rectangular box as illustrated in Figure 3. The heating element and the micro heat exchanger were both placed horizontally inside the box. The setup, which included the experimental section and the auxiliary devices, is shown in Figure 4. It consisted of a thermostatic bath to supply the test section with pure water in the first step at an inlet temperature (T_{in}) ranging from 25 °C to 65 °C and TiO_2/water nanofluids in the same temperature range in the second step. The nanofluid was circulated through the micro heat exchanger using a variable-speed prostate pump. A data acquisition system was used for the display and storage of all parameters measured.

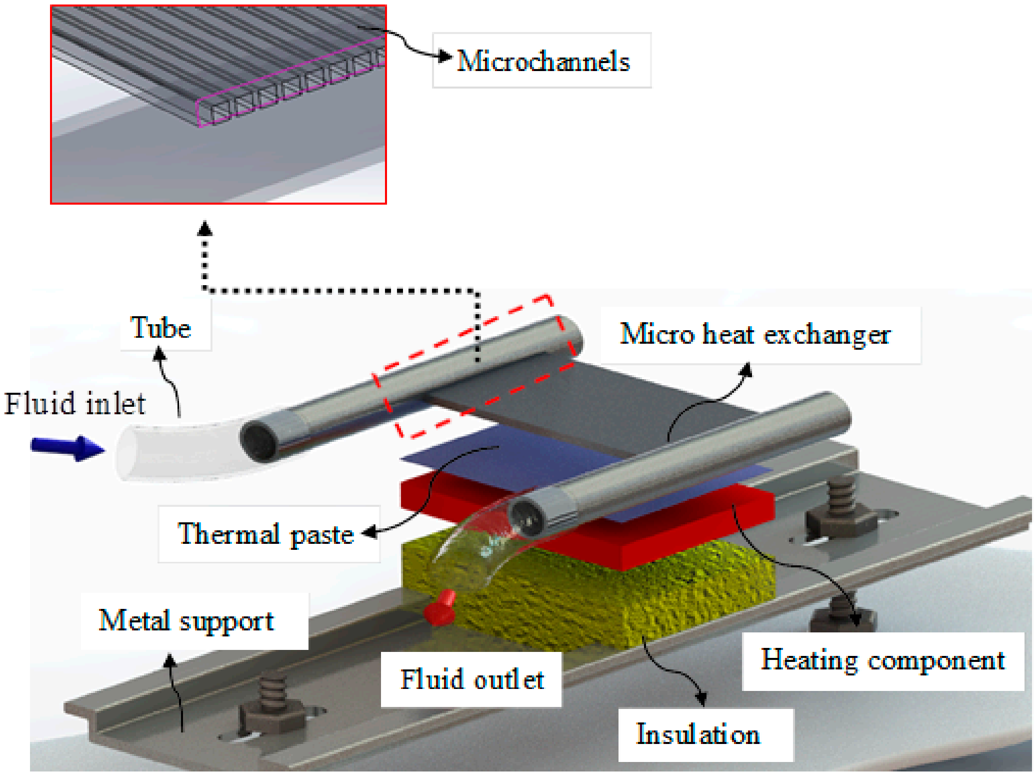

Figure 4. Embedded device in parallelepiped box.

Temperatures were recorded using thermocouples placed at eight different positions on the experimental device, as depicted in Figure 5. Three thermocouples were installed in the micro heat exchanger at the inlet (T1), outlet (T2), and middle of the outer surface (T3). Two thermocouples were installed in ambient air, namely, T7 and the thermostatic bath (T8). Three additional thermocouples were installed at 20 mm intervals along the length of the microchannel. A data acquisition system and a computer were used to monitor the temperature sensors and to register data at 10 s intervals. The distribution of these temperature sensors in the experimental setup is shown in Figure 5. The total pressure drop in the micro heat exchanger was measured employing a 0–2 bar pressure meter. The voltage regulator was fixed at its maximum value of 220 V at the start of the experiment, yielding a power supply of 100 W. The experiment was run for 30 min at a pure water flow rate of 0.1 L/min. The experiment was then repeated at water flow rates ranging from 0.1 to 0.5 L/min, corresponding to Reynolds numbers in the range of 400–2000. The inlet water temperature varied between 35 °C and 65 °C. The room temperature throughout the experimental phase varied from 24 °C to 26 °C, as several heat-generating equipment supplies were active.

The same experimental procedure was carried out again under the same conditions for the nanofluids. The heat component was cooled before starting the next experiment. It was necessary to pretreat and clean the inner surfaces of the microchannels with pure water to remove nanoparticles before each experiment.

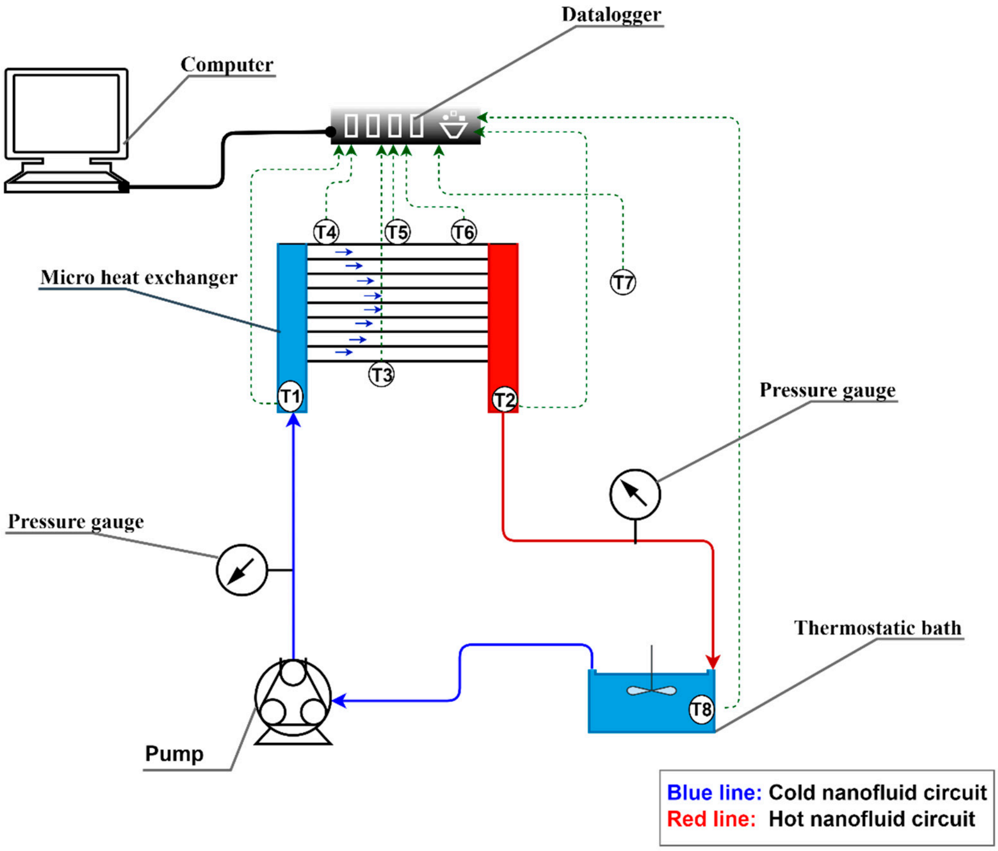

Figure 5. Codification of the thermocouples installed in the experimental setup.

2.3. Nanofluid Preparation and Calculation of Thermophysical Properties

Pure water and TiO_2 were used as the base fluid and nanomaterial, respectively. The thermophysical properties of the TiO_2 nanoparticles are summarized in Table 2. The TiO_2/water nanofluids were formulated with TiO_2 nanoparticles at mass concentrations of 0%, 1%, and 5%, which were dispersed and stirred in water (refer to Figure 6 for details). The TiO_2 nanoparticles were initially mixed using a magnetic stirrer operating at a rotation speed of 700 rpm for 4–5 h to ensure thorough dispersion and to prevent significant precipitation. Subsequently, the stirred nanofluids underwent ultrasonication using a 200 W, 45 kHz digital sonicator for approximately 5 h to achieve optimal dispersion. The stability of the nanosuspension solution was assessed at two volume fractions of nanoparticles, ϕ = 1% and 5%, to evaluate the effectiveness of the dispersion process and the overall stability of the nanofluids.

Table 2. Thermophysical properties of TiO_2 nanoparticles [53–55].

Properties	TiO_2 Nanoparticles
Mean diameter, dp	20 nm
Thermal conductivity, k	8.4 W/m.K
Specific heat, Cp	710 J/kg.K
Density, ρ	4157 kg/m^3

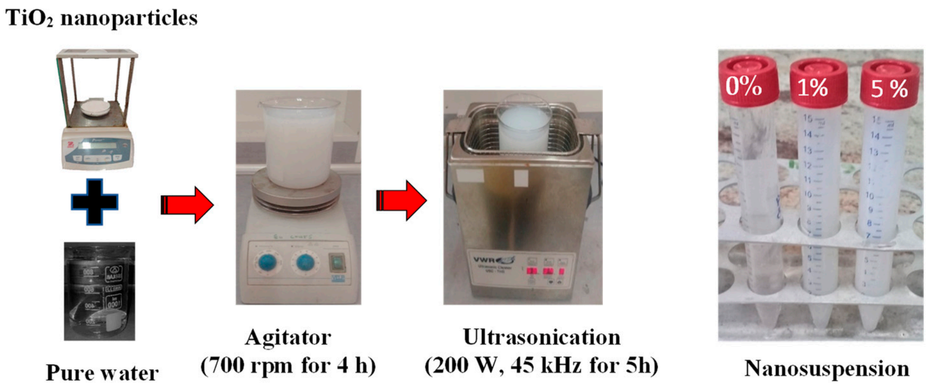

Figure 6. Depicts the preparation process of the TiO_2-based nanofluids at different concentrations.

The volume concentration of nanofluids from the given weight fraction of nanoparticles is calculated by the following equation [56]:

$$\varnothing = \frac{m_{np} \times \rho_{bf}}{\left(\rho_{np} \times (1 - m_{np}) + m_{np} \times \rho_{bf}\right.} \tag{2}$$

The thermophysical properties of the nanofluids, such as density (ρ), heat capacity (C_P), dynamic viscosity (μ_f), and thermal conductivity (k), were evaluated using the correlations proposed and defined as follows [57–60]:

- Density of nanofluids:

$$\rho_{nf} = \varnothing\rho_{np} + (1 - \varnothing)\rho_{nf} \tag{3}$$

- Specific heat of nanofluids:

$$C_{Pnf} = \frac{\varnothing\rho_{np}C_{Pnp} + \left(1 - \varnothing\right)\rho_{bf}}{\rho_{nf}} \tag{4}$$

- Viscosity of nanofluids:

$$\mu_{nf} = \frac{\mu_{nf}}{(1 - \varnothing)^{2.5}} \tag{5}$$

- Thermal conductivity of nanofluids:

$$k_{nf} = k_{bf}\left[\frac{k_{np} + (n-1)k_{bf} - (n-1)\varnothing\left(k_{bf} - k_{np}\right)}{k_{np} + (n-1)k_{bf} + \varnothing\left(k_{bf} - k_{np}\right)}\right] \tag{6}$$

where $n = 3$ for the spherical-shaped nanoparticles.

3. Data Reduction in the Experimental Data

3.1. Heat Transfer

The heat transfer and overall heat transfer coefficient of the convection test section are expressed as follows:

$$\dot{Q} = \dot{m}C_P(T_{int} - T_{out}) = h_{avg}A_{eff}\ LMTD \tag{7}$$

$$h_{avg} = \frac{\dot{Q}}{A_{eff}\ LMTD} \tag{8}$$

The log-mean temperature difference ($LMTD$) through the micro heat exchanger is calculated by Equation (9), as follows:

$$LMTD = \frac{(T_{s,max} - T_{int}) - (T_{s,max} - T_{out})}{ln\frac{(T_{s,max}\ -\ T_{int})}{(T_{s,max}\ -\ T_{out})}} \tag{9}$$

A_{eff} is the wetted channel area, which is expressed as follows:

$$A_{eff} = 2\ (H_{mc}\ + W_{mc})\ L\ N \tag{10}$$

The Nusselt number is calculated by Equation (11), as follows:

$$Nu_{avg} = \frac{h_{avg}\ D_h}{k} \tag{11}$$

The thermal resistance is defined as the ratio from the temperature difference between the heating element and the water at the entrance to the heating element power supplied (Equation (12)), as follows:

$$R_{th} = \frac{T_{s,max} - T_{int}}{Q} \tag{12}$$

where $T_{s,max}$ is the maximum surface temperature of the heat sink.

3.2. Fluid Flow

The Reynolds number is defined by Equation (13), using the hydraulic diameter and the inlet velocity through the micro channel, as follows:

$$R_e = (\rho \times V_{max} \times D_h)/\mu \tag{13}$$

Hydraulic diameter is expressed by Equation (14), as follows:

$$D_h = \frac{2 \times (H_{mc} \times W_{mc})}{(H_{mc} + W_{mc})} \tag{14}$$

The velocity of the V_{mc} can be calculated by the following equation:

$$\dot{V}_{in} = n\ V_{mc}\ A_{mc} \tag{15}$$

while n and A_{mc} represent, respectively, the number of flow microchannels and the cross-sectional area of each flow channel, as given by:

$$A_{mc} = H_{mc} \times W_{mc} \tag{16}$$

Pressure drops in the microchannel, ΔP, can be calculated from the pressure drop measured between the inlet and outlet, using the following equation:

$$\Delta P = P_{exp} - \rho g LOSS_{minor} \tag{17}$$

where

$$LOSS_{minor} = Enlargement\ LOSS + Contraction\ LOSS \tag{18}$$

This is illustrated in the schematic diagrams of the micro heat exchanger in Figures 4 and 5.

The total minor losses were calculated based on the losses resulting from expansion and contraction in the different sections, as follows [61]:

$$\Delta P = \frac{\rho V_{mc}^2}{2}\left((2K_{90})\left(\frac{A_{mc}}{A_c}\right)^2 + (K_e + K_c) + \frac{4f_{app}L_{mc}}{D_h}\right) + \left(\rho V_{tube}^2\left(\frac{4f_{tube}L_{tube}}{D_{tube}}\right)\right) + \frac{\rho V_{tube}^2}{2}\left(\frac{A_{tube}}{A_c}\right)^2 + (K_{e\ int} + K_{c\ out}) \tag{19}$$

A_{mc} and A_c represent the total cross-sectional area of the microchannels and the collector, respectively. K_{90} is the loss coefficient for the 90-degree bends that occur between the collector inlet on the entrance side of the microchannels and the bend formed by the collector outlet on the exit side of the microchannels. A value of 1.2 was recommended for this coefficient [61]. K_e and K_c represent contraction and expansion loss coefficients caused by area changes [61], and their values can be estimated from graphical data for a square channel [61]. These coefficients are determined based on the ratio between the channel area and the collector flow area (A_{mc}/A_c), where A_{tube} and V_{tube} represent, respectively, the area $(\pi D^2/4)$ and velocity $(\dot{V}_{in}/A_{tube})$ of the male run tee union tube. The friction factor, f_{tube}, can be analytically calculated using the Poiseuille equation, as follows: $f_{tube} = 64/Re$

The loss coefficients for the sudden expansion (K_{e_int}) and the sudden contraction (K_{c_out}) represent the pressure losses that occur, respectively, as a result of the sudden expansion between the tube outlet and collector inlet (K_{c_out}), and the sudden contraction between the collector outlet and tube inlet (K_{e_int}). These coefficients can be determined from the correlations reported by Idelchik [62], as follows:

$$K_{e\_int} = \left(1 - \frac{A_{tube}}{A_c}\right) \text{ and } K_{c\_out} = 0.4\left(1 - \frac{A_{tube}}{A_c}\right) \tag{20}$$

Regarding the value of f_{app} for the development of laminar flow regimes, it was calculated using data reported in Reference [61].

Constant pumping power:

$$\dot{W} = \dot{V}\Delta P \tag{21}$$

3.3. Performance Evaluation Criterion (PEC)

A performance evaluation criterion (PEC) was used [63] to evaluate the heat transfer enhancement using nanofluids in a micro heat exchanger. This parameter represents the ratio between the increase in heat transfer and the increase in pumping power required for the system (Equation (22)). A system with a PEC ≤ 1 is not recommended, as it requires more energy for pumping power than the improvement in the heat transfer process. However, if PEC > 1, the gain in heat transfer is more significant than the increase in energy required for pumping power, so the system could be feasible for heat transfer enhancement in practical applications.

$$PEC = \frac{\left(\frac{Nu_{nf}}{Nu_{bf}}\right)}{\left(\frac{f_{nf}}{f_{bf}}\right)^{\frac{1}{3}}} \tag{22}$$

3.4. Uncertainty of the Experimental Data

The two types of uncertainty, Type A and Type B, correspond to the different sources of error encountered in the experiment. Type A uncertainty, u_A, is associated with the statistical method used in data analysis and includes random errors or fluctuations in the data. This type of uncertainty can be estimated using statistical methods, such as the standard deviation or standard error of the mean. Type B uncertainty, u_B, is associated with the accuracy of the experimental instruments and includes systematic errors or biases in the data. The total uncertainty (U) of the experimental data is calculated using the following formula [64]:

$$U = \sqrt{u_A^2 + \sum_{j+1}^{n} u_{B.j}^2} \tag{23}$$

where

$$u_A = \sqrt{\sum_{i=1}^{i=n} (xi - \overline{x})2/[n(n-1)]} \tag{24}$$

$$u_B = \frac{\delta}{\lambda} \tag{25}$$

where $\overline{x}$ is the average of the values measured, xi is the actual value measured, and n is the times at which the value was measured. δ is half the width of the possible interval of the value measured, and λ is the coverage factor.

Considering that a result, R, is calculated from a set of quantities measured, x_i, $R = (x_1, x_2, x_3, \ldots, x_i)$; then, the uncertainty of the value calculated is as follows [64]:

$$U_R = \sqrt{\sum_{i=1}^{n} \left(\left(\frac{\partial R}{\partial x_i} \right) U\,(x_i) \right)^2} \tag{26}$$

Table 3 summarizes the uncertainty of the various sensors used in the experiments, and the parameters are calculated with a confidence level of 95%.

Table 3. Uncertainties of the various sensors used in the experiments, as well as the parameters calculated.

Sensor	Uncertainty
K-type thermocouple	±0.1 °C
Pressure sensors	±2.5% FS
Peristaltic pump	±1%
Heater power supply voltage and current	0.01% and 0.1%
L (mm)	2.5
W (mm)	1.25
Parameter	**Uncertainty (%)**
Re	1.54
ΔP (Pa)	0.5
h ($W/m^2 \cdot °C$)	2
Nu	3

4. Numerical Approach

This section presents the physical model used in the simulation analysis of the monophasic flow in the micro heat exchanger [65]. The governing equations, boundary conditions, and meshing required for the numerical simulation are provided. Figure 7A depicts the configuration of the micro heat exchanger evaluated in the present study. The calculation model considered an elementary volume, shown in Figure 7B. Computational Fluid Dynamics (CFD) ANSYS/FLUENT 14.0, employing the finite volume approach [66] was used to simulate the conjugate heat transport within the microchannels.

4.1. Assumptions and Boundary Conditions

The cooling performance of the micro heat exchanger was investigated employing a three-dimensional fluid–solid model. The following assumptions were made in the model: (i) incompressible, laminar, and steady state flow; (ii) constant properties of solids and fluids; (iii) neglected effects of gravity in the momentum equation and viscous dissipation in the energy equation; and (iv) adiabatic external surface boundaries, except on the bottom of the micro heat exchanger.

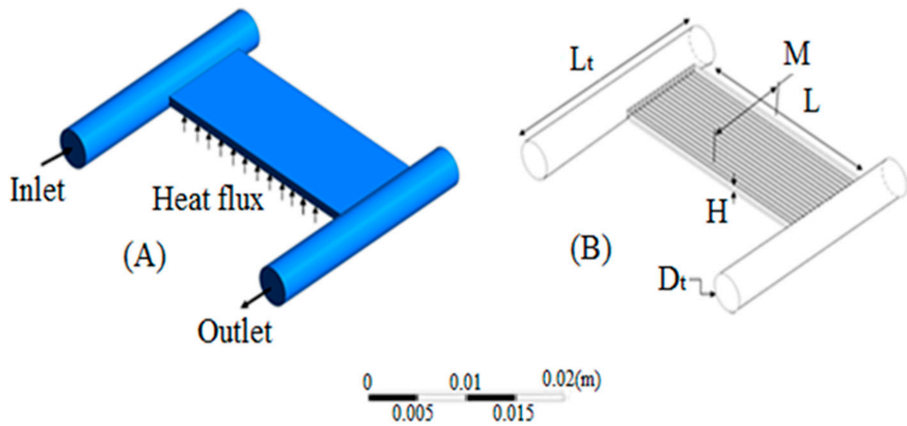

Figure 7. Micro heat exchanger: (**A**) layout; (**B**) calculation volume.

Numerical simulations were run using water at temperatures (T_{in}) between 25 °C and 65 °C at the collector entrance and water Reynolds numbers ranging from 400 to 2000. The heating power applied to the bottom of the micro heat exchanger was 100 W. A second-order upwind approach was employed to solve the energy and momentum equations, and the SIMPLE algorithm was applied to manage the coupling of the pressure force fields and velocity. The walls between solid and liquid regions were designated interfaces, and the inlet and outlet walls of the microchannels were taken as inner walls. The remaining walls were considered adiabatic walls. The iterative procedure was regarded as successful when the residuals of the continuity and momentum equations were below 10^{-4} and those of the energy equations were lower than 10^{-7}.

4.2. Governing Equations

The governing equations employed in the model are the standard continuity equations for mass conservation, the Navier–Stokes equation for momentum conservation, and the energy equation to predict the conjugate heat transfer. The assumptions mentioned above were established in order to construct the following governing differential equations for fluid flow and heat transfer, as follows:

- Continuity equation:

$$\nabla\left(\rho_{nf}\, V\right) = 0 \tag{27}$$

- Momentum conservation equation:

$$\rho_{\,nf}(v \times \nabla V) = -\nabla P + \nabla\left(\mu_{\,nf} \nabla V\right) \tag{28}$$

- Energy conservation equation:

$$\rho_{nf} C_{nf}\; v \times \nabla T = k_{nf} \nabla^2 T \tag{29}$$

4.3. Effect of Grid Refinement

The mesh density was analyzed before carrying out the final simulations to determine how it influenced the numerical solution for the entire micro heat exchanger. The green dotted line indicates a critical threshold for mesh density in the mesh sensitivity analysis. Accordingly, different numerical trials were performed for several numbers of mesh elements between 6×10^5 and 2×10^6 to ensure the independency of the mesh size. The heating element temperature and the total pressure were used to assess how the mesh number affected the accuracy of the results. Figure 8 illustrates the mesh sensitivity analysis performed at a Reynolds number of 400, an input heat power of 100 W, and an inlet cooling nanofluid temperature of 25 °C. It can be observed that the results were not affected when the number of mesh elements was above 14×10^5.

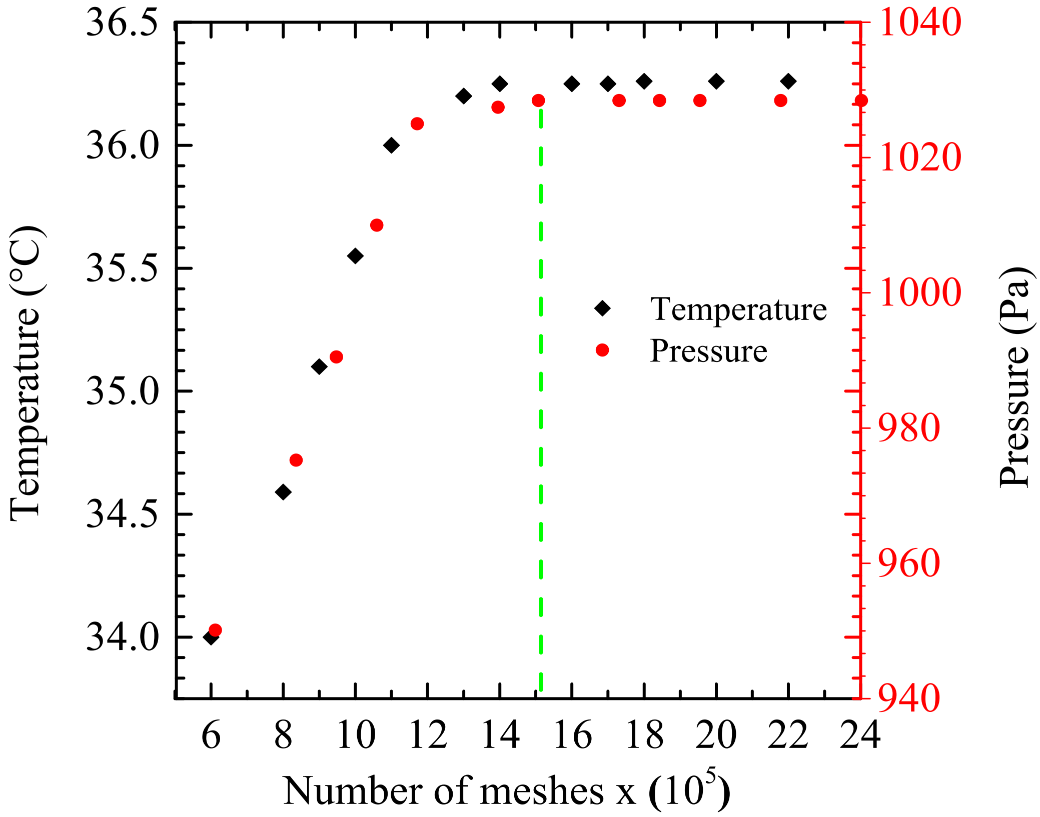

Figure 8. Influence of the grid size on the temperature variation along the microchannels centerline.

5. Results and Discussion

This section reports the results of how heat transfer in cooling electronic components is enhanced when a micro heat exchanger and warm nanofluids are employed. Both experimental and numerical results are presented with nanoparticle concentrations ranging from 1% to 5% in weight. The effects of the inlet temperature and the nanoparticle concentrations of hot nanofluids on the cooling of electronic components are discussed. First, both the experimental setup and the numerical simulation tool were validated. Pure water was used, and the validation considered the correlations and experimental data of the heat transfer and pressure drop for laminar flows in rectangular microchannels reported in the literature [67–74].

5.1. Validation of Experimental Results

To validate the experimental setup and procedure, initial test runs were carried out on the micro heat exchanger at an inlet temperature of 25 °C, five Reynolds numbers, and a power input of 100 W. The Nusselt number and friction factor were used as validation parameters. The experimental results of the present study on heat transfer were compared with the experimental data reported by Lee et al. [67], and the values predicted by the Peng and Peterson correlation [68], as shown in Equation (30).

$$Nu = 0.1165\left(\frac{D_h}{W_c}\right)^{0.81}\left(\frac{H}{W}\right)^{-0.79} Re^{0.62} Pr^{\frac{1}{3}} \quad for\ \ Re < 2200 \tag{30}$$

where H and W are the height and width of the microchannel, respectively, and W_c is the center-to-center distance between microchannels

Figure 9 shows the comparison commented above in terms of the Nusselt number versus the Reynolds number when using pure water. The deviations between the experimental data carried out for the present work and those reported by Lee et al. [67] are 14% at Re = 400. This discrepancy decreases progressively to 2% as the Reynolds number increases to Re = 2000. Regarding the comparison between the experimental data of the current study and the values predicted by the Peng and Peterson correlation [68], the deviation is less than 2% for a Reynolds number of 400 and increases continuously as the Reynolds number increases, until it reaches 5% at Re = 2000.

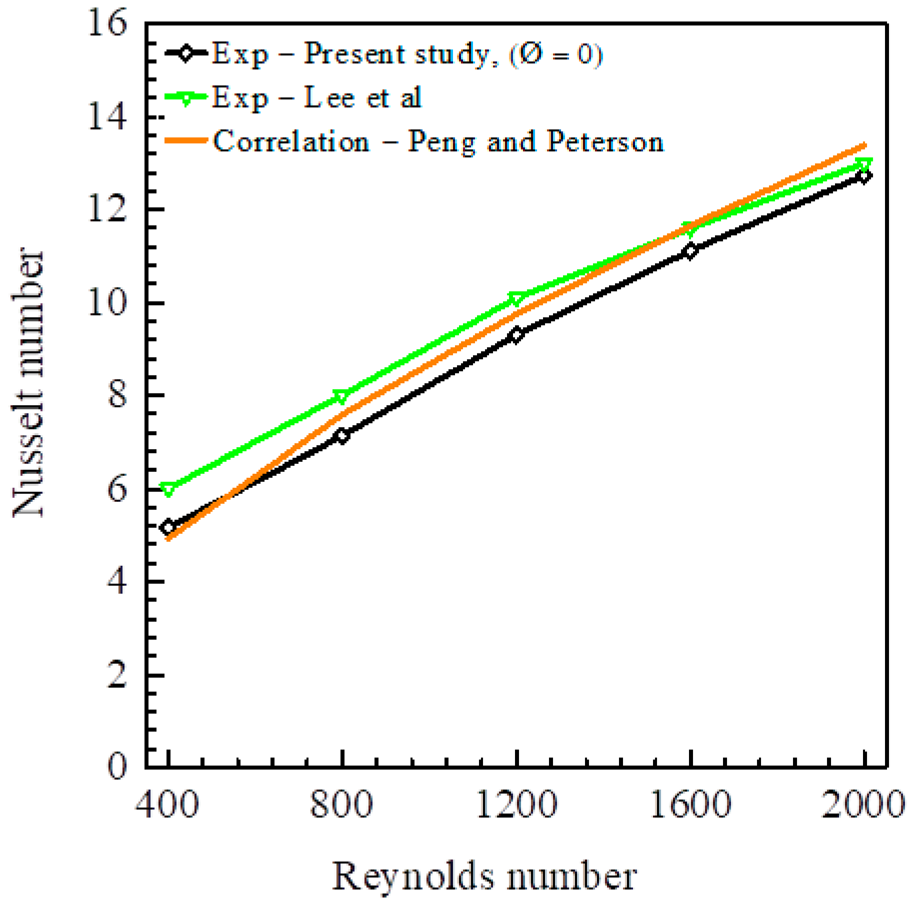

Figure 9. Comparison of the average Nusselt number with the experimental data of Lee et al. [67] and the values calculated by the Peng and Peterson correlation, using pure water [68].

The authors compared the experimental results of the present study for rectangular microchannels, as shown in Figure 10. The friction factor was compared with the values predicted by the correlation of Shah and London [69] and with the experimental data reported by Harms et al. [70]. Shah and London [69] proposed the correlation, presented in Equation (31), to predict the pressure drop for developed laminar flows inside rectangular channels.

$$P_0 = 24\left(1 - 1.3553\alpha + 1.9467\alpha^2 - 1.7012\alpha^3 + 0.9564\alpha^4 - 0.2537\alpha^5\right) \quad (31)$$

where $\alpha = \frac{W_{mc}}{H_{mc}}$ is the channel aspect ratio.

Figure 10 shows the comparison commented above at a cooling water inlet temperature of 25 °C. All sets of data present a similar trend, with a sharp decrease for Reynolds numbers ranging from 400 to 800 and after a less pronounced variation at higher values of the Reynolds number. The mean absolute deviation between the experimental data of the present work and the values predicted by the correlation of Shah and London [69] is around 10%. The minimum and maximum deviations between the experimental data of Harms et al. [70] and those of the present work are 3% and 25%, respectively.

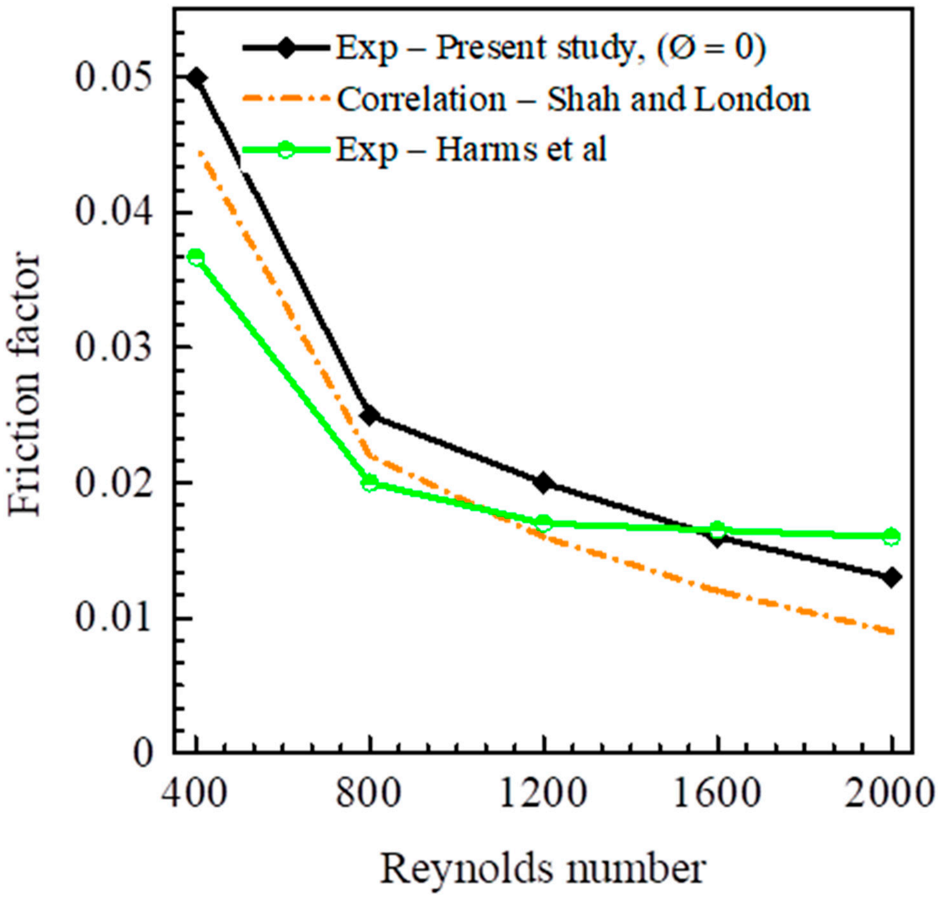

Figure 10. Comparison of the friction factor with the experimental data of Harms et al. [70] and the values calculated by the Shah and London correlation [69].

5.2. Validation of the Simulation Code

To validate the simulation code developed, the values of thermal resistance obtained in the present work were compared with the experimental data reported by Kawano et al. [71] and the numerical results of Qu and Mudawar [72] and Al-Neama et al. [73], as shown in Figure 11. This comparison was carried out for Reynolds numbers ranging from 80 to 400 and at an inlet cooling water temperature of 20 °C. A constant heat flux of 100 W/cm^2 was applied to the bottom wall of the micro heat exchanger. The maximum deviation between the numerical values of the present work and the numerical data of Al-Neama et al. [73] is about 6%. With respect to the experimental and numerical data reported by Kawano et al. [71] and Qu and Mudawar [72], the maximum deviations are 10% and 11%, respectively.

On the basis of the analysis presented above, it may be concluded that the experimental and numerical results obtained with the micro heat exchanger used in the present work are well in agreement with the results reported in the literature. This validates both the experimental and numerical approaches developed by the authors.

5.3. Heat Transfer Characteristics

The experimental work investigated the Nusselt number achieved in the micro heat exchanger versus the Reynolds number at a hot nanofluid inlet temperature ranging from 35 °C to 65 °C and at three nanoparticle concentrations, namely, 0%, 1%, and 5%, as shown in Figure 12. The Reynolds number varied between 400 and 2000, while the power dissipated by the electronic heating component was kept constant at $\dot{P}$ = 100 W. The Nusselt number increased and the heat transfer process improved at higher values of the Reynolds number. Additionally, because of an increase in the thermal conductivity, the heat transfer process was enhanced by the addition of TiO_2 nanoparticles to the pure water (i.e., base fluid). Table 4 presents the heat transfer enhancement with the addition of nanoparticles to pure water at Reynolds numbers of 400, 800, 1200, and 2000 and a nanofluid inlet temperature ranging from 35 °C to 65 °C at intervals of 10 K.

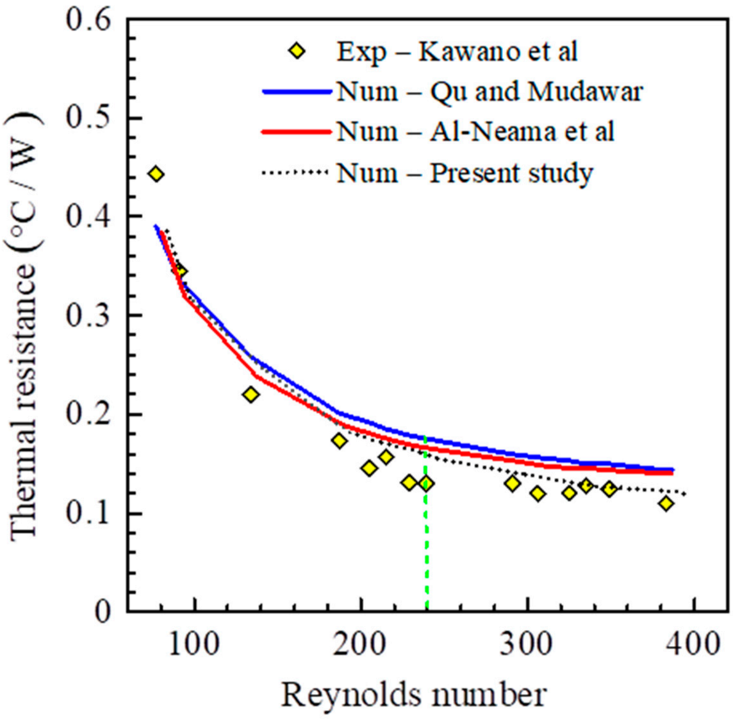

Figure 11. Comparison of the numerical results with data reported by Kawano et al. [71], Qu and Mudawar [72], and Al-Neama et al. [73].

With the lower Reynolds number (Re = 400), the heat transfer enhancement was around 21–25% at a nanoparticle concentration of 1% for all the values considered for the nanofluid inlet temperature. This enhancement increases to 32–36% at a nanoparticle concentration of 5%. There was a continuous improvement in the heat transfer as the Reynolds number increased. The highest value reached for heat transfer enhancement was 70%. This was achieved at a Reynolds number of 2000, a nanoparticle concentration of 5%, and a nanofluid inlet temperature of 35 °C. The results also show how significantly the nanofluid inlet temperature affects heat transfer. This may be attributed to the fact that the boundary layer becomes thinner due to the decrease in viscosity as the nanofluid temperature increases [74]. Therefore, a heat transfer enhancement value of 4–8% was observed when the nanofluid inlet temperature decreased from 65 °C to 55 °C. Heat transfer enhancement was around 8–10% and 10–17% when the nanofluid inlet temperature decreased from 65 °C to 45 °C and from 65 °C to 35 °C, respectively.

As commented above, to operate safely, the target is for the cooling system to maintain the temperature of the electronic heating components below the limit of 80 °C. For safety, the temperature (T_{cs}) is then set at 70 °C [72].

Additionally, the temperature profile of the heating components was analyzed versus the Reynolds number and nanoparticle concentration at nanofluid inlet temperatures ranging from 35 °C to 65 °C at intervals of 10 K, as depicted in Figure 13. As observed in this figure, the increase in both the Reynolds number and the nanoparticle concentration lowers the temperature of the heating components. This facet widens the safety margin for temperature to a critical limit of 80 °C. The maximum temperature difference between the electronic heating component and the critical limit of 80 °C was around 37.4 °C for pure water, 38.6 °C at $\varnothing$ = 1%, and 39.5 °C at $\varnothing$ = 5%. At nanofluid inlet temperatures of 45 °C and 55 °C, the temperature of the electronic heating components remains below the safety limit. As the nanoparticle concentration increases, the temperature of the electronic heating components was reduced, as shown in Figure 13b,c. The heat transfer enhancement was substantiated by adding nanoparticles to pure water. However, at an inlet temperature of 65 °C, the operating temperature of the electronic equipment was above the safety temperature limit established (i.e., 70 °C), even with the addition of nanoparticles or an increase in the Reynolds number, as shown in Figure 13d.

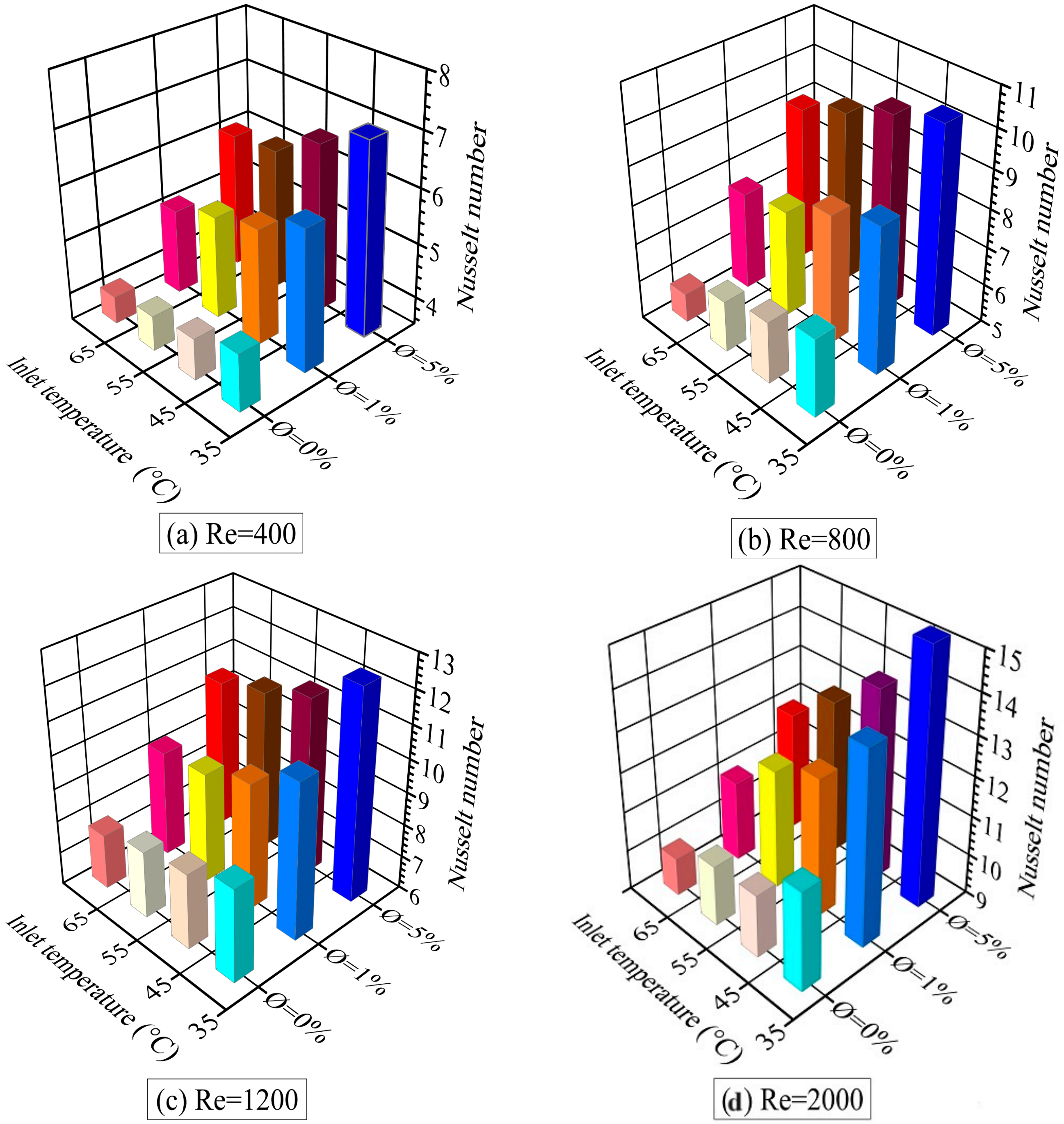

Figure 12. Average Nusselt number versus nanofluid concentration and inlet temperature at different Reynolds numbers: (**a**) Re = 400; (**b**) Re = 800; (**c**) Re = 1200; (**d**) Re = 1600.

Table 4. Heat transfer enhancement in the micro heat exchanger due to the addition of nanoparticles to pure water.

Φ (%)	**1**				**5**			
Re \ **T_{in} (°C)**	**35**	**45**	**55**	**65**	**35**	**45**	**55**	**65**
400	26%	24%	23%	21%	37%	35%	32%	30%
800	35%	32%	30%	28%	52%	49%	47%	45%
1200	44%	42%	40%	39%	60%	57%	55%	53%
2000	57%	56%	54%	49%	70%	65%	63%	59%

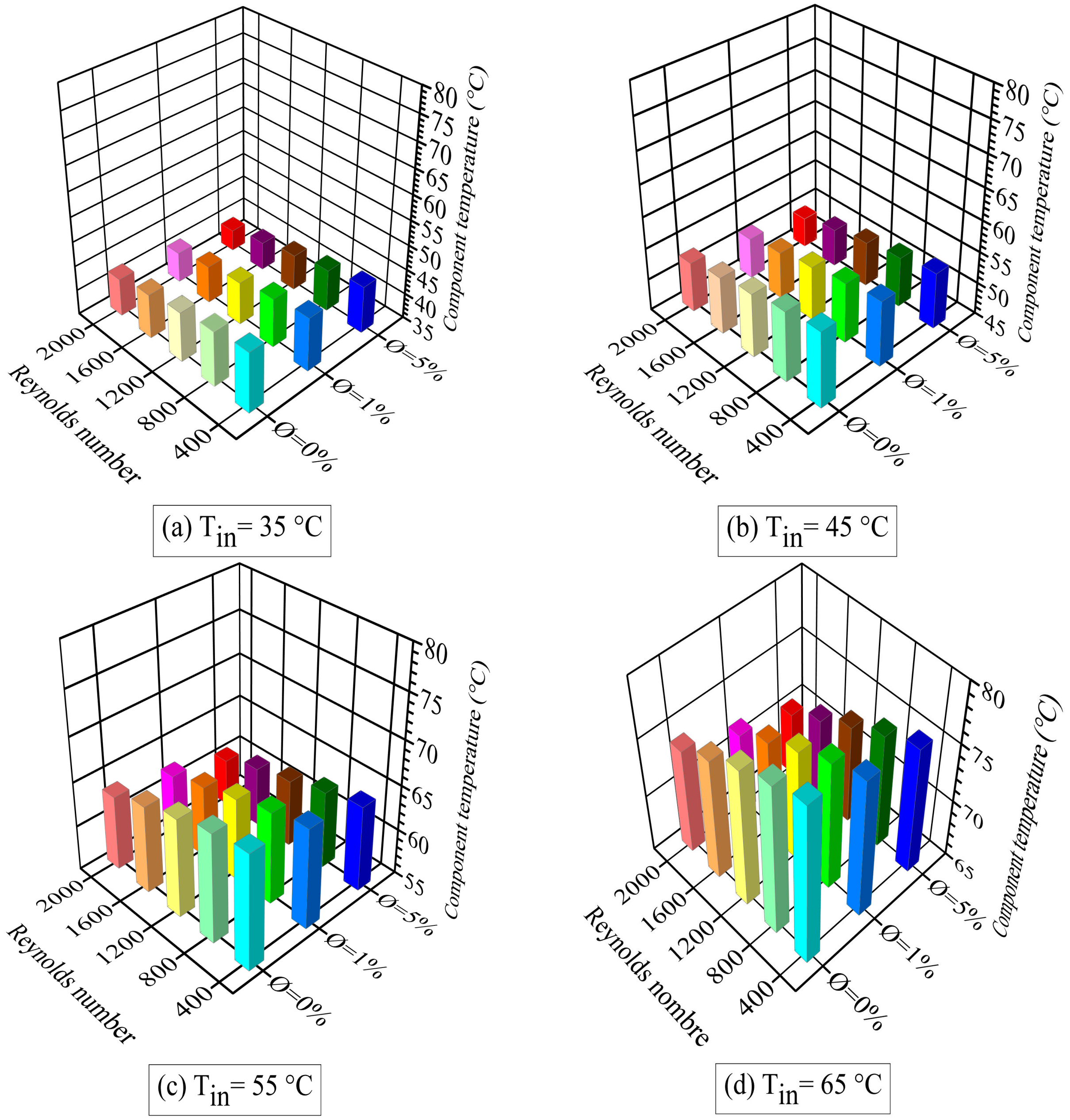

Figure 13. Temperature profile of the heating component versus the Reynolds number and the nanoparticle concentration at different nanofluid inlet temperatures: (**a**) T_{in} = 35 °C; (**b**) T_{in} = 45 °C; (**c**) T_{in} = 55 °C; (**d**) T_{in} = 65 °C.

Figure 14 illustrates the nanofluid temperature distribution through a contour inside the micro heat exchanger at mass nanoparticle concentrations of 0, 1, and 5% in weight, a Reynolds number of Re = 1200, and an inlet temperature of 45 °C. This figure shows the impact of the nanoparticle concentration on nanofluid temperature profiles inside the micro heat exchanger. For pure water (Figure 14a), the fluid temperature reaches 51 °C in the middle of the heat sink and 54 °C near the outlet of the microchannel. At a 1% nanoparticle concentration (Figure 14b), these two temperatures are 49 °C and 52 °C, respectively. Regarding the case of a 5% nanoparticle concentration (Figure 14c), the corresponding temperatures are 47 °C and 50 °C, respectively. The results indicate that there is a difference in performance between employing pure water and nanofluids, with the difference becoming more significant as the concentration of TiO_2 nanoparticles is increased. The CFD simulations performed on the micro heat exchanger further support these trends.

5.4. Pressure Drop Characteristics

Figure 15 shows the pressure drop in the micro heat exchanger as a function of the Reynolds number at three mass fractions of TiO_2 nanoparticles, namely, ϕ = 0% (pure water), ϕ = 1%, and ϕ = 5%. Both experimental and numerical results are presented in this figure. The pressure drop was significantly higher as the Reynolds number increased. The use of nanoparticles moderately increased the pressure drop at a given Reynolds number. This is because nanofluids have a higher viscosity than pure water. It is worthy of note that the maximum deviations between the experimental data and the numerical predictions were in the range 6.2–6.7% for the three mass fractions used. The maximum value of the pressure drop was obtained with nanofluids at a 5% nanoparticle concentration and a Reynolds number of 2000. A pressure drop increase of about 20% was observed for the use of TiO_2/water nanofluids compared to that of base fluid (i.e., pure water).

Figure 16 shows the pumping power required in the micro heat exchanger for pure water and for nanofluids at 1% and 5% of nanoparticle concentrations. The pumping power increases almost linearly with the Reynolds number. The effect of nanoparticle concentrations on the pumping power is more significant at high Reynolds numbers because nanofluids have a higher density and viscosity than pure water.

5.5. Performance Evaluation Analysis

Figure 17 shows the performance evaluation criterion (PEC) parameter versus the Reynolds number and the nanofluid inlet temperature at nanoparticle concentrations of 1% and 5%. The PEC parameter is always greater than the unity for both nanoparticle concentrations. This demonstrates that adding nanoparticles to cooling water circulating in a micro heat exchanger improves heat transfer process. A better heat transfer performance was obtained with a 5% nanoparticle concentration at an Re = 2000 and a T_{in} = 35 °C (PEC = 1.45). At nanofluid inlet temperatures of 45 °C and 55 °C, the PEC parameter decreased to 1.41 and 1.38, respectively.

At a nanoparticle concentration of 1%, the PEC parameter was equal to 1.36 when the Reynolds number and the inlet temperature were set to 2000 and 35 °C, respectively. When the nanofluid inlet temperature and the Reynolds number were set to 65 °C and 2000, respectively, the PEC parameter decreased to 1.02–1.10 for both nanoparticle concentrations considered. This reveals that heat transfer enhancement due to the addition of nanoparticles is more pronounced than the resulting increase in pumping power required.

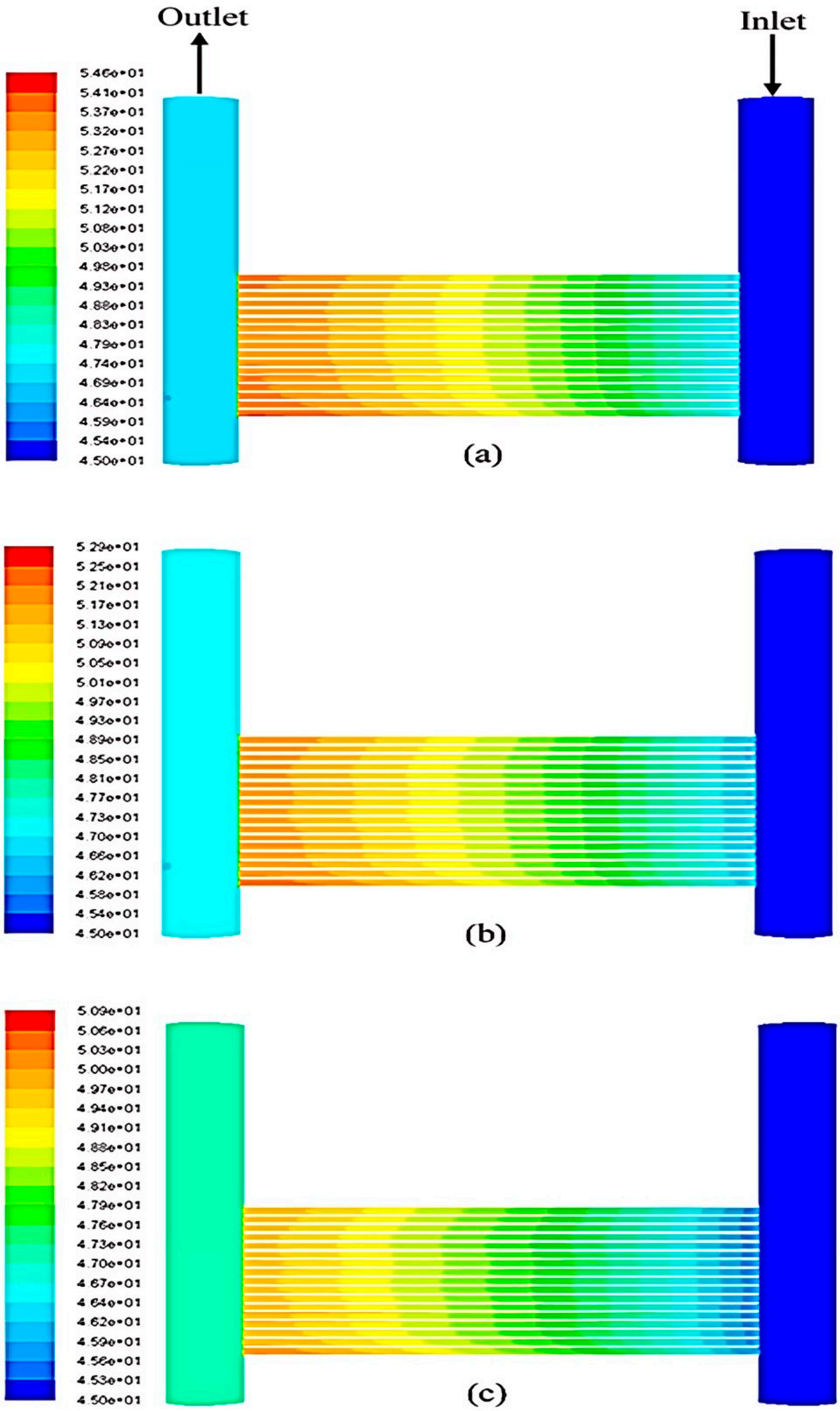

Figure 14. Temperature contours (°C) at Re = 1200, inlet temperature of 45 °C, and different nanoparticle concentrations: (**a**) pure water; (**b**) Ø = 1%; (**c**) Ø = 5%.

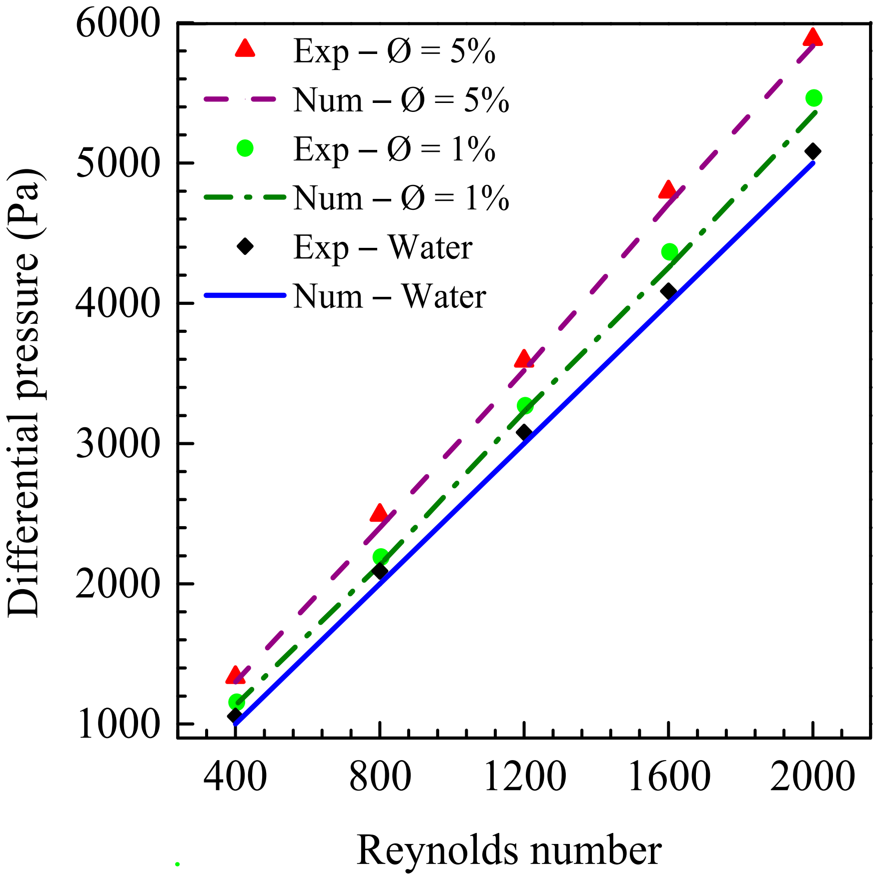

Figure 15. Pressure drops versus the Reynolds number for both TiO_2 nanofluids and pure water.

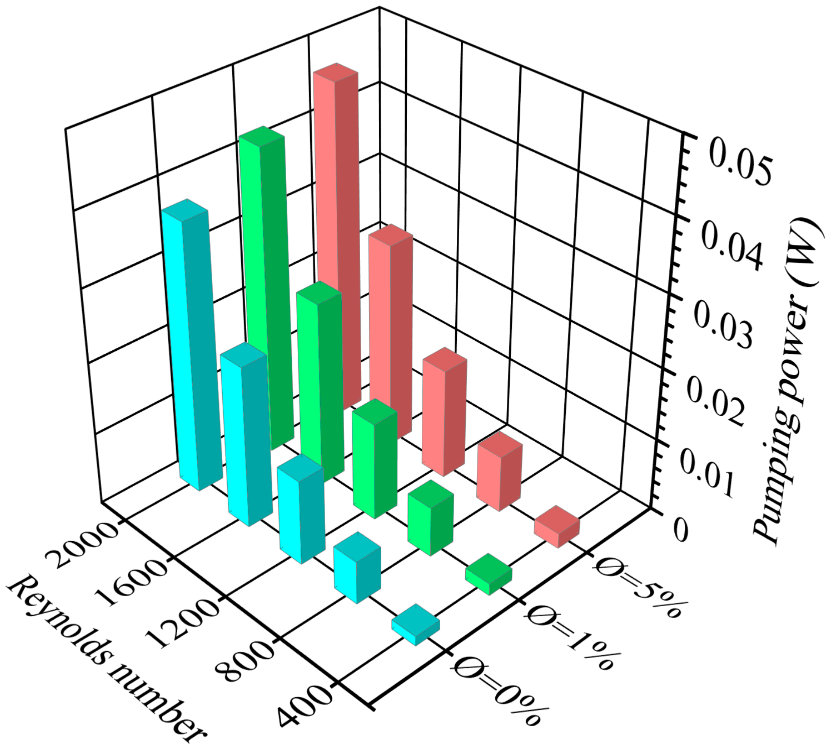

Figure 16. Pumping power versus the Reynolds number for both TiO_2 nanofluids and pure water.

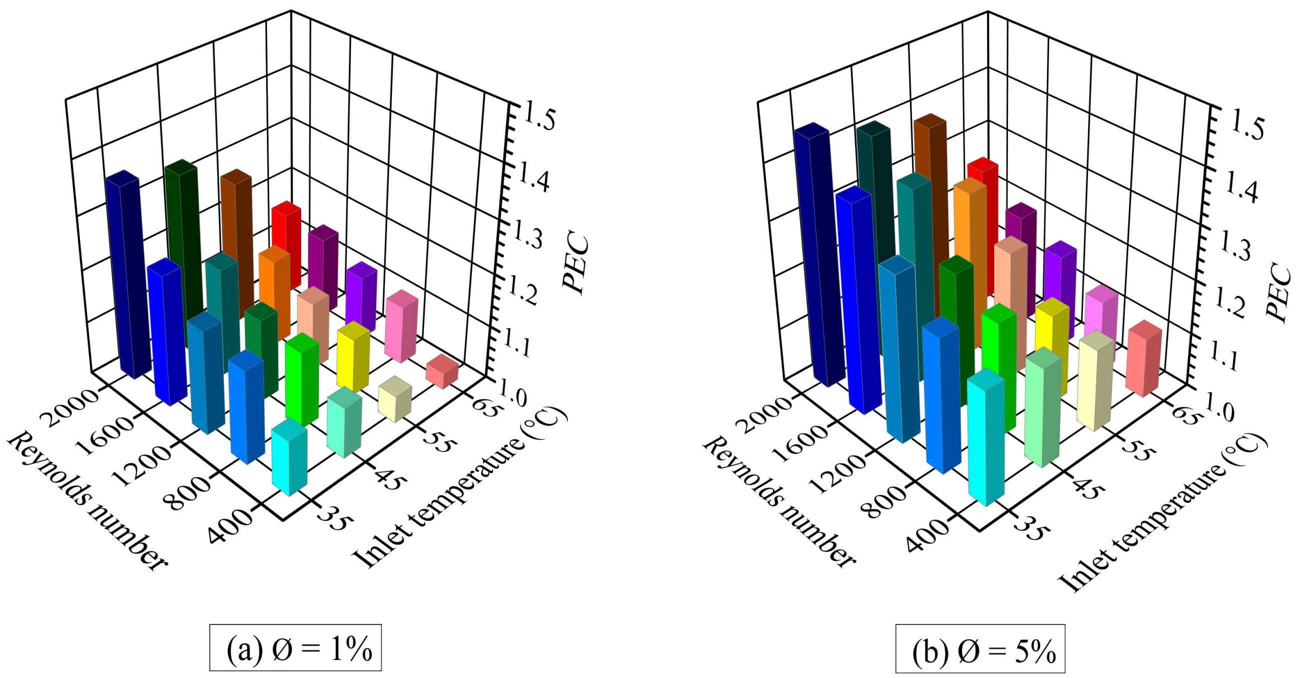

Figure 17. Performance evaluation criterion (PEC) versus the Reynolds number and nanofluid inlet temperature at two TiO_2 concentrations: (**a**) Ø = 1%; (**b**) Ø = 5%.

6. Conclusions

Heat transfer enhancement, in a micro heat exchanger, using titanium dioxide (TiO_2) for cooling electronic components at high coolant inlet temperatures was investigated both experimentally and numerically. A micro heat exchanger was built and tested in the cooling mode employing TiO_2/water nanofluids at mass fractions of 1% and 5%, Reynolds numbers ranging from 400 to 2000, and inlet temperatures ranging between 35 °C and 65 °C at 10 °C intervals. A constant and uniform heat load of 100 W was supplied to the channel from the bottom of the exchanger. The maximum operating temperature allowed for electronic components is 80 °C. The effect of the nanoparticle concentrations, Reynolds numbers, and inlet temperatures of the nanofluids on the cooling of the electronic components was analyzed using three parameters, namely, the Nusselt number, friction factor, and performance evaluation criterion (PEC). The main results are summarized below:

- Both the experimental setup and the numerical simulation tool were validated using pure water, correlations, and experimental data on heat transfer and pressure drops as reported in the literature for laminar flows in rectangular microchannels. The deviations between the Nusselt number and the friction factor from the present work and those from the literature were between 2% and 25%.
- An enhancement in the heat transfer process was obtained with the addition of TiO_2 nanoparticles to pure water (i.e., base fluid), on account of the increase in thermal conductivity. At a nanofluid inlet temperature of 55 °C and a nanoparticle concentration of 1%, the Nusselt number increased by 23% to 54% as the Reynolds number varied between 400 and 2000. At a nanoparticle concentration of 5%, the corresponding percentages for Nusselt enhancement were 32% and 63%. The highest value of heat transfer enhancement achieved was 70%, which occurred at a Reynolds number of 2000, a nanoparticle concentration of 5%, and an inlet nanofluid temperature of 35 °C.
- It was observed that the nanofluid inlet temperature significantly affected the heat transfer. A heat transfer enhancement of about 10% was obtained when the nanofluid inlet temperature decreased from 65 °C to 45 °C.
- The increase in both the Reynolds number and the nanoparticle concentration lowered the temperature of the heating components. This widened the safety margin for the

critical temperature limit of 80 °C. However, at an inlet temperature of 65 °C, the operating temperature of the electronic equipment was above the safety temperature limit set at 70 °C, even with the addition of nanoparticles and applying high Reynolds numbers.

- The maximum value of the pressure drop was obtained with nanofluids at a 5% nanoparticle concentration and a Reynolds number of 2000. A pressure drop increase of about 20% was observed when using (TiO_2/water) nanofluids instead of base fluid (i.e., pure water).
- The PEC values were always greater than the unity for both nanoparticle concentrations. This indicates that adding nanoparticles to cooling water circulating in a micro heat exchanger improves the heat transfer process. At a Reynolds number of 2000 and a nanofluid inlet temperature of 35 °C, PEC values of 1.36 and 1.45 were obtained for nanoparticle concentrations of 1% and 5%, respectively. When the nanofluid inlet temperature increased to 65 °C, the PEC parameter decreased to 1.02–1.10 for both concentrations.

Author Contributions: M.M.: Conceptualization, Methodology, Software, Validation, Formal Analysis, Investigation, and Writing—Original Draft; M.B.: Conceptualization, Methodology, Formal Analysis, Writing—Review and Editing, Supervision, and Project Administration. All authors have read and agreed to the published version of the manuscript.

Funding: Mahdi Mokrane gratefully acknowledges the EPST/Renewable Energy Development Center (CDER) of Algeria for funding his internships at Rovira i Virgili University of Tarragona (Spain).

Data Availability Statement: The data presented in this paper is available upon request from the correspond author.

Conflicts of Interest: The authors declare no conflict of interest.

Nomenclature

A_{eff}	Effective heat transfer area (m^2)
A_c	Collector area (m^2)
A_{mc}	Cross-sectional area of each flow channel (m^2)
A_{tube}	Tube area (m^2)
C_p	Specific heat (J/kg.K)
d_p	Particle diameter (nm)
D_c	Collector diameter (mm)
D_h	Hydraulic diameter (mm)
e	Thickness of pin fin (mm)
e_s	Thickness of the upper face of the heat sink (mm)
f_{app}	Apparent friction factor
h	Convective heat transfer coefficient (W/m^2.K)
H	Heat sink depth (mm)
H_{mc}	Microchannel depth (mm)
k	Thermal conductivity (W/m.K)
K_c	Contraction loss coefficient
K_e	Expansion loss coefficient
K_{90}	Bend loss coefficient (=1.2)
I	Electrical intensity (A)
L_c	Collector tube length (mm)
L	Heat sink length (mm)
m	Mass (kg)
N	Number of channels
Nu	Nusselt number
P	Pressure (Pa)

$\dot{P}$	Electric power (W)
$\dot{Q}$	Heat transfer rate (W)
Re	Reynolds Number
Pr	Prandtl number
t	Time (s)
T	Temperature (°C)
u, v, and w	Velocity in the directions x, y, and z (m/s)
$\dot{U}$	Voltage (V)
$\dot{V}$	Volume flow (m^3/s)
W	Heat sink width (mm)
$\dot{W}$	Power pumping (W)
Symbols	
ρ	Density (kg/m^3)
μ	Dynamic viscosity (kg/m.s)
γ	Convergence criterion
ϕ	Particle mass fraction (%)
λ	Coverage factor
α	Channel aspect ratio
$LMTD$	Log-mean temperature difference (°C)
PEC	Performance evaluation criterion
Subscripts	
avg	Average
bf	Base fluid
c	Collector
in	Inlet
f	Fluid
mc	Microchannel
min	Minimum
max	Maximum
nf	Nanofluid
np	Nanoparticle
out	Outlet
s	Surface

References

1. Zimmermann, S.; Tiwari, M.K.; Meijer, I.; Paredes, S.; Michel, B.; Poulikakos, D. Hot water-cooled electronics: Exergy analysis and waste heat reuse feasibility. *Int. J. Heat Mass Transf.* **2012**, *55*, 6391–6399. [CrossRef]
2. Zhang, H.Y.; Pinjala, D.; Wong, T.N.; Toh, K.C.; Joshi, Y.K. Single-phase liquid cooled microchannel heat sink for electronic packages. *Appl. Therm. Eng.* **2005**, *25*, 1472–1487. [CrossRef]
3. Naphon, P.; Wiriyasart, S. Liquid cooling in the mini-rectangular fin heat sink with and without thermoelectric for CPU. *Int. Commun. Heat Mass Transf.* **2009**, *36*, 166–171. [CrossRef]
4. Tuckerman, D.B.; Pease, R.F.W. High-Performance Heat Sinking for VLSI. *IEEE Electron Device Lett.* **1981**, *EDL-2*, 126–129. Available online: https://ieeexplore.ieee.org/document/1481851 (accessed on 10 November 2017). [CrossRef]
5. Gao, P.; Le Person, S.; Favre-Marinet, M. Scale effects on hydrodynamics and heat transfer in two-dimensional mini and microchannels. *Int. J. Therm. Sci.* **2002**, *41*, 1017–1027. [CrossRef]
6. Mala, G.M.; Li, D. Flow characteristics of water in microtubes. *Int. J. Heat Fluid Flow* **1999**, *20*, 142–148. [CrossRef]
7. Fedorov, A.G.; Viskanta, R. Three-dimensional conjugate heat transfer in the microchannel heat sink for electronic packaging. *Int. J. Heat Mass Transf.* **2000**, *43*, 399–415. [CrossRef]
8. Wu, H.Y.; Cheng, P. Friction factors in smooth trapezoidal silicon microchannels with different aspect ratios. *Int. J. Heat Mass Transf.* **2003**, *46*, 2519–2525. [CrossRef]
9. Colgan, E.G.; Furman, B.; Gaynes, A.; Graham, W.; LaBianca, N.; Magerlein, J.H.; Polastre, R.J.; Rothwell, M.B.; Bezama, R.J. A practical implementation of silicon microchannel coolers for high power chips. *IEEE Trans. Compon. Packag. Technol.* **2007**, *30*, 218–225. Available online: https://ieeexplore.ieee.org/document/4214931 (accessed on 29 February 2020). [CrossRef]
10. Hong, F.; Cheng, P. Three dimensional numerical analyses and optimization of offset strip-fin microchannel heat sinks. *Int. Commun. Heat Mass Transf.* **2009**, *36*, 651–656. [CrossRef]
11. Foong, A.J.L.; Ramesh, N.; Chandratilleke, T.T. Laminar convective heat transfer in a microchannel with internal longitudinal fins. *Int. J. Therm. Sci.* **2009**, *48*, 1908–1913. [CrossRef]

12. Xie, Y.; Shen, Z.; Zhang, D.; Lan, J. Thermal performance of a water-cooled microchannel heat sink with grooves and obstacles. *J. Electron. Packag. Trans. ASME* **2014**, *136*, 021001. [CrossRef]
13. Gholami, H.; Banaei, M.; Eskandari, A. Investigation of effect of triangular rib in heat transfer of finned rectangular microchannel with extended surfaces. *Life Sci. J.* **2013**, *10*, 206–211. Available online: http://www.Lifesciencesite.com (accessed on 18 January 2018).
14. Muzychka, Y.S. Constructal design of forced convection cooled microchannel heat sinks and heat exchangers. *Int. J. Heat Mass Transf.* **2005**, *48*, 3119–3127. [CrossRef]
15. Bello-Ochende, T.; Liebenberg, L.; Meyer, J.P. Constructal cooling channels for micro-channel heat sinks. *Int. J. Heat Mass Transf.* **2007**, *50*, 4141–4150. [CrossRef]
16. Salimpour, M.R.; Sharifhasan, M.; Shirani, E. Constructal optimization of the geometry of an array of micro-channels. *Int. Commun. Heat Mass Transf.* **2011**, *38*, 93–99. [CrossRef]
17. Bello-Ochende, T.; Meyer, J.P.; Ighalo, F.U. Combined numerical optimization and constructal theory for the design of microchannel heat sinks. *Numer. Heat Transf. Part A Appl.* **2010**, *58*, 882–899. [CrossRef]
18. Olakoyejo, O.T.; Bello-Ochende, T.; Meyer, J.P. Mathematical optimisation of laminar forced convection heat transfer through a vascularized solid with square channels. *Int. J. Heat Mass Transf.* **2012**, *55*, 2402–2411. [CrossRef]
19. Olakoyejo, O.T.; Bello-Ochende, T.; Meyer, J.P. Constructal conjugate cooling channels with internal heat generation. *Int. J. Heat Mass Transf.* **2012**, *55*, 4385–4396. [CrossRef]
20. Bejan, A. Constructal-theory network of conducting paths for cooling a heat generating volume. *Int. J. Heat Mass Transf.* **1997**, *40*, 799–811. [CrossRef]
21. Kumar, S.; Kumar, A.; Kothiyal, A.D.; Bisht, M.S. A review of flow and heat transfer behaviour of nanofluids in micro channel heat sinks. *Therm. Sci. Eng. Prog.* **2018**, *8*, 477–493. [CrossRef]
22. Zimmermann, S.; Meijer, I.; Tiwari, M.K.; Paredes, S.; Michel, B.; Poulikakos, D. Aquasar: A hot water-cooled data center with direct energy reuse. *Energy* **2012**, *43*, 237–245. [CrossRef]
23. Sarafraz, M.M.; Hormozi, F. Experimental study on the thermal performance and efficiency of a copper made thermosyphon heat pipe charged with alumina-glycol based nanofluids. *Powder Technol.* **2014**, *266*, 378–387. [CrossRef]
24. Nojoomizadeh, M.; Karimipour, A. The effects of porosity and permeability on fluid flow and heat transfer of multi walled carbon nano-tubes suspended in oil (MWCNT/Oil nano-fluid) in a microchannel filled with a porous medium. *Phys. E Low-Dimens. Syst. Nanostruct.* **2016**, *84*, 423–433. [CrossRef]
25. Saravanan, K.; Ravishankar, P.; Sivakumar, V.; Velmurugan, K. Review of heat transfer and fluid flow of nanofluids. *Renew. Sustain. Energy Rev.* **2017**, *78*, 460–482.
26. Gupta, S.K.; Gupta, S.; Gupta, T.; Raghav, A.; Singh, A. A review on recent advances and applications of nanofluids in plate heat exchanger. *Mater. Today Proc.* **2021**, *44*, 229–241. [CrossRef]
27. Godson, L.; Raja, B.; Lal, D.M.; Wongwises, S. Enhancement of heat transfer using nanofluids-An overview. *Renew. Sustain. Energy Rev.* **2010**, *14*, 629–641. [CrossRef]
28. Murshed, S.M.S.; Nieto de Castro, C.A.; Lourenço, M.J.V.; Lopes, M.L.M.; Santos, F.J.V. A review of boiling and convective heat transfer with nanofluids. *Renew. Sustain. Energy Rev.* **2011**, *15*, 2342–2354. [CrossRef]
29. Sundar, L.S. Synthesis and characterization of hybrid nanofluids and their usage in different heat exchangers for an improved heat transfer rate: A critical review. *Eng. Sci. Technol. Int. J.* **2023**, *44*, 101468. [CrossRef]
30. Kim, T.I.; Jeong, Y.H.; Chang, S.H. An experimental study on CHF enhancement in flow boiling using Al_2O_3 nano-fluid. *Int. J. Heat Mass Transf.* **2010**, *53*, 1015–1022. [CrossRef]
31. Wu, J.M.; Zhao, J. A review of nanofluid heat transfer and critical heat flux enhancement—Research gap to engineering application. *Prog. Nucl. Energy* **2013**, *66*, 13–24. [CrossRef]
32. Porgar, S.; Oztop, H.F.; Salehfekr, S. A comprehensive review on thermal conductivity and viscosity of nanofluids and their application in heat exchangers. *J. Mol. Liq.* **2023**, *386*, 122213. [CrossRef]
33. Ahmed, W.; Kazi, S.N.; Chowdhury, Z.Z.; Johan, M.R.B.; Akram, N.; Mujtaba, M.A.; Gul, M.; Oon, C.S. Experimental investigation of convective heat transfer growth on ZnO@TiO_2/DW binary composites/hybrid nanofluids in a circular heat exchanger. *J. Therm. Anal. Calorim.* **2020**, *143*, 879–898. [CrossRef]
34. Fang, X.; Chen, Y.; Zhang, H.; Chen, W.; Dong, A.; Wang, R. Heat transfer and critical heat flux of nanofluid boiling: A comprehensive review. *Renew. Sustain. Energy Rev.* **2016**, *62*, 924–940. [CrossRef]
35. Salman, B.H.; Mohammed, H.A.; Munisamy, K.M.; Kherbeet, A.S. Characteristics of heat transfer and fluid flow in microtube and microchannel using conventional fluids and nanofluids: A review. *Renew. Sustain. Energy Rev.* **2013**, *28*, 848–880. [CrossRef]
36. Daungthongsuk, W.; Wongwises, S.A. Critical review of convective heat transfers of nanofluids. *Renew. Sustain. Energy Rev.* **2007**, *11*, 797–817. [CrossRef]
37. Ahmed, W.; Chowdhury, Z.Z.; Kazi, S.N.; Johan, M.R.; Akram, N.; Oon, C.S. Effect of ZnO-water based nanofluids from sonochemical synthesis method on heat transfer in a circular flow passage. *Int. Commun. Heat Mass Tranfer* **2020**, *114*, 104591. [CrossRef]
38. Hussein, A.M.; Sharma, K.V.; Bakar, R.A.; Kadirgama, K. A review of forced convection heat transfer enhancement and hydrodynamic characteristics of a nanofluid. *Renew. Sustain. Energy Rev.* **2014**, *29*, 734–743. [CrossRef]

39. Hussien, A.A.; Abdullah, M.Z.; Al-Nimr, M.A. Single-phase heat transfer enhancement in micro/minichannels using nanofluids: Theory and applications. *Appl. Energy* **2016**, *164*, 733–755. [CrossRef]
40. Kakaç, S.; Pramuanjaroenkij, A. Review of convective heat transfer enhancement with nanofluids. *Int. J. Heat Mass Transf.* **2009**, *52*, 3187–3196. [CrossRef]
41. Yu, W.; France, D.M.; Timofeeva, E.V.; Singh, D.; Routbort, J.L. Comparative review of turbulent heat transfer of nanofluids. *Int. J. Heat Mass Transf.* **2012**, *55*, 5380–5396. [CrossRef]
42. Sundar, L.S.; Singh, M.K. Convective heat transfer and friction factor correlations of nanofluid in a tube and with inserts: A review. *Renew. Sustain. Energy Rev.* **2013**, *20*, 23–35. [CrossRef]
43. Mohammed, H.A.; Bhaskaran, G.; Shuaib, N.H.; Saidur, R. Heat transfer and fluid flow characteristics in microchannels heat exchanger using nanofluids: A review. *Renew. Sustain. Energy Rev.* **2011**, *15*, 1502–1512. [CrossRef]
44. Vanaki, S.M.; Ganesan, P.; Mohammed, H.A. Numerical study of convective heat transfer of nanofluids: A review. *Renew. Sustain. Energy Rev.* **2016**, *54*, 1212–1239. [CrossRef]
45. Sabaghan, A.; Edalatpour, M.; Moghadam, M.C.; Roohi, E.; Niazmand, H. Nanofluid flow and heat transfer in a microchannel with longitudinal vortex generators: Two-phase numerical simulation. *Appl. Therm. Eng.* **2016**, *100*, 179–189. [CrossRef]
46. Lee, J.; Mudawar, I. Assessment of the effectiveness of nanofluids for single-phase and two-phase heat transfer in micro-channels. *Int. J. Heat Mass Transf.* **2007**, *50*, 452–463. [CrossRef]
47. Kalteh, M.; Abbassi, A.; Saffar-Avval, M.; Frijns, A.; Darhuber, A.; Harting, J. Eulerian–Eulerian two-phase numerical simulation of nanofluid laminar forced convection in a microchannel. *Int. J. Heat Fluid Flow* **2011**, *32*, 107–116. [CrossRef]
48. Mohammed, H.A.; Gunnasegaran, P.; Shuaib, N.H. Heat transfer in rectangular microchannels heat sink using nanofluids. *Int. Commun. Heat Mass Transf.* **2010**, *37*, 1496–1503. [CrossRef]
49. Manay, E.; Sahin, B. The effect of microchannel height on performance of nanofluids. *Int. J. Heat Mass Transf.* **2016**, *95*, 307–320. [CrossRef]
50. Martínez, V.A.; Vasco, D.A.; García-Herrera, C.M.; Ortega-Aguilera, R. Numerical study of TiO_2-based nanofluids flow in microchannel heat sinks: Effect of the Reynolds number and the microchannel height. *Appl. Therm. Eng.* **2019**, *161*, 114130. [CrossRef]
51. Nitiapiruk, P.; Mahian, O.; Dalkilic, A.S.; Wongwises, S. Performance characteristics of a microchannel heat sink using TiO_2/water nanofluid and different thermophysical models. *Int. Commun. Heat Mass Transf.* **2013**, *47*, 98–104. [CrossRef]
52. Heydari, M.; Toghraie, D.; Akbari, O.A. The effect of semi-attached and offset mid-truncated ribs and Water/TiO_2 nanofluid on flow and heat transfer properties in a triangular microchannel. *Therm. Sci. Eng. Prog.* **2017**, *2*, 140–150. [CrossRef]
53. Bouanimba, N.; Laid, N.; Zouaghi, R.; Sehili, T. A Comparative Study of the Activity of TiO_2 Degussa P25 and Millennium PCs in the Photocatalytic Degradation of Bromothymol Blue. *Int. J. Chem. React. Eng.* **2017**, *16*, 20170014. [CrossRef]
54. Laid, N.; Bouanimba, N.; Ben Ahmede, A.; Toureche, A.; Sehili, T. Characterization of ZnO and TiO_2 Nanopowders and their Application for Photocatalytic Water Treatment. *Acta Phys. Pol. A* **2020**, *137*, 305–312. [CrossRef]
55. Ebrahimnia-Bajestan, E.; Charjouei Moghadam, M.; Niazmand, H.; Daungthongsuk, W.; Wongwises, S. Experimental and numerical investigation of nanofluids heat transfer characteristics for application in solar heat exchangers. *Int. J. Heat Mass Transf.* **2016**, *92*, 1041–1052. [CrossRef]
56. Arshad, W.; Ali, H.M. Experimental investigation of heat transfer and pressure drop in a straight minichannel heat sink using TiO_2 nanofluid. *Int. J. Heat Mass Transf.* **2017**, *110*, 248–256. [CrossRef]
57. Pak, B.C.; Cho, Y.I. Hydrodynamic and heat transfer study of dispersed fluids with submicron metallic oxide particles. *Exp. Heat Transf.* **1998**, *11*, 151–170. [CrossRef]
58. Xuan, Y.; Roetzel, W. Conceptions for heat transfer correlation of nanofluids. *Int. J. Heat Mass Transf.* **2000**, *43*, 3701–3707. [CrossRef]
59. Rea, U.; McKrell, T.; Hu, L.W.; Buongiorno, J. Laminar convective heat transfers and viscous pressure loss of alumina-water and zirconia-water nanofluids. *Int. J. Heat Mass Transf.* **2009**, *52*, 2042–2048. [CrossRef]
60. Gonçalves, I.; Souza, R.; Coutinho, G.; Miranda, J.; Moita, A.; Pereira, J.E.; Moreira, A.; Lima, R. Thermal Conductivity of Nanofluids: A Review on Prediction Models, Controversies and Challenges. *Appl. Sci.* **2021**, *11*, 2525. [CrossRef]
61. Kandlikar, S.G. Single-phase liquid flow in minichannels and microchannels. In *Heat and Fluid Flow in Minichannels and Microchannels*; Elsevier: Amsterdam, The Netherlands, 2006; pp. 87–136. [CrossRef]
62. Idelchik, I.E. *Handbook of Hydraulic Resistance*; Hemisphere Publishing: New York, NY, USA, 1986.
63. Zhang, J.; Diao, Y.; Zhao, Y.; Zhang, Y. An experimental investigation of heat transfer enhancement in minichannel: Combination of nanofluid and micro fin structure techniques. *Exp. Therm. Fluid Sci.* **2017**, *81*, 21–32. [CrossRef]
64. Moffat, R.J. Describing the uncertainties in experimental results. *Exp. Therm. Fluid Sci.* **1988**, *1*, 3–17. [CrossRef]
65. Mokrane, M.; Lounis, M.; Announ, M.; Ouali, M.; Djebiret, M.A.; Bourouis, M. Performance analysis of a micro heat exchanger in electronic cooling applications. *J. Therm. Eng.* **2021**, *7*, 773–790. Available online: https://jten.yildiz.edu.tr/article/34 (accessed on 2 February 2022). [CrossRef]
66. Patankar, S.V. *Numerical Heat Transfer and Fluid Flow*; CRC Press: Boca Raton, FL, USA, 1980. [CrossRef]
67. Lee, P.S.; Garimella, S.V.; Liu, D. Investigation of heat transfer in rectangular microchannels. *Int. J. Heat Mass Transf.* **2005**, *48*, 1688–1704. [CrossRef]

68. Peng, X.F.; Peterson, G.P. Convective heat transfer and flow friction for water flow in microchannel structures. *Int. J. Heat Mass Transf.* **1996**, *39*, 2599–2608. [CrossRef]
69. Shah, R.K.; London, A.L. *Laminar Flow Forced Convection in Ducts: A Source Book for Compact Heat Exchanger Analytical Data*; Academic Press: New York, NY, USA, 1978. [CrossRef]
70. Harms, T.M.; Kazmierczak, M.J.; Gerner, F.M. Developing convective heat transfer in deep rectangular microchannels. *Int. J. Heat Fluid Flow* **1999**, *20*, 149–157. [CrossRef]
71. Kawano, K.; Sekimura, M.; Minakami, K.; Iwasaki, H.; Ishizuka, M. Development of micro channel heat exchanging. *JSME Int. J. Ser. B Fluids Therm. Eng.* **2001**, *44*, 592–598. [CrossRef]
72. Qu, W.; Mudawar, I. Experimental and numerical study of pressure drop and heat transfer in a single-phase micro-channel heat sink. *Int. J. Heat Mass Transf.* **2002**, *45*, 2549–2565. [CrossRef]
73. Al-Neama, A.F.; Kapur, N.; Summers, J.; Thompson, H.M. An experimental and numerical investigation of the use of liquid flow in serpentine microchannels for microelectronics cooling. *Appl. Therm. Eng.* **2017**, *116*, 709–723. [CrossRef]
74. Kumar, V.; Sarkar, J. Experimental hydrothermal behavior of hybrid nanofluid for various particle ratios and comparison with other fluids in minichannel heat sink. *Int. Commun. Heat Mass Transf.* **2020**, *110*, 104397. [CrossRef]